Journal of Alloys and Compounds 588 (2014) 534–539

Contents lists available at ScienceDirect

Journal of Alloys and Compounds

journal homepage: www.elsevier.com/locate/jalcom

Effect of Fe substitution on electrochemical properties of $Sn_{3.95}Fe_{0.05}P_3$ alloy anode for lithium ion batteries

Gumjae Park [a,*], Chulho Lee [a], Jueun Lee [a], Joon Hwan Choi [b], Yun-Sung Lee [c], Sang-Min Lee [a,*]

[a] Battery Research Center, Korea Electrotechnology Research Institute, 12 Bulmosan-ro 10beon-gil, Changwon 642-120, Republic of Korea
[b] Powder and Ceramics Division, Korea Institute of Materials Science, 797 Changwondaero, Changwon 642-831, Republic of Korea
[c] Faculty of Applied Chemical Engineering, Chonnam National University, 300 Yongbong-dong, Gwangju 500-757, Republic of Korea

ARTICLE INFO

Article history:
Received 9 July 2013
Received in revised form 11 October 2013
Accepted 14 November 2013
Available online 22 November 2013

Keywords:
$Sn_{3.95}Fe_{0.05}P_3$ alloy
Sn_4P_3 alloy
Fe substitution
Transition metal phosphide
Anode
Lithium ion batteries

ABSTRACT

$Sn_{3.95}Fe_{0.05}P_3$ alloy was synthesized via a solvothermal method, using tin metal, iron metal and amorphous red phosphorous. The XRD and TEM results showed that Fe ion was successfully substituted on original the Sn_4P_3 layered structure without any structure changes. The $Sn_{3.95}Fe_{0.05}P_3$ alloy anode showed a higher initial charge capacity and coloumbic efficiency of 1304 mAh g^{-1} and 73% compared with the Sn_4P_3 alloy anode, respectively. Additionally, a relatively large capacity of about 420 mAh g^{-1} after 100th cycles was achieved in the $Sn_{3.95}Fe_{0.05}P_3$ anode, whereas the capacity of the Sn_4P_3 anode remained at only about 100 mAh g^{-1} after 100 cycles. Fe atoms as an inactive matrix could be dispersed between the tin atoms, resulting in the suppression of tin agglomeration in $Sn_{3.95}Fe_{0.05}P_3$ during cycling. It is confirmed from the voltage profile and differential capacity plots that the Fe ion in the $Sn_{3.95}Fe_{0.05}P_3$ structure could stabilize the structure and improve the electrochemical properties during cycling.

1. Introduction

Over the past few decades, lithium ion batteries (LIBs) have been considered as power sources of portable devices due to their high energy density, light weight and long life cycle [1]. More recently, the use of LIBs has expanded to large-scale power applications in the hybrid Electric Vehicle (HEV) and Energy Storage System (ESS), taking advantage of their high energy density. However, it is necessary to improve the properties of LIBs in order to satisfy commercial needs. The limited capacity and safety issue of anode materials used in the electrode materials for LIBs restrict the output of energy density for the battery, thus disrupting its attractiveness in large-scale power applications. The commercial graphite anode is limited to the specific capacity of 372 mAh g^{-1}, with increasing energy density of LIB is impeded [2–5]. Moreover, graphite anode has a low operating potential, close to that of Li^+/Li, thus inducing critical safety problems due to the risk of lithium dendrite formation during lithium intercalation [6–9]. Recently, many studies have been undertaken to search alternative anode materials to those of carbonaceous materials. Metal phosphides (MP_x: M = Sn [10–13], Mn [14,15], Fe [16–18] and Co [19–21], [22–26]) have been considered as possible candidates for anode materials in lithium ion batteries because of their high capacities at relatively low potentials. In addition, the major operating voltage of metal phosphide is higher than the voltage of lithium deposition, resulting in a reduced risk of lithium dendrite. Depending on the metal, metal phosphides can be categorized according to two reaction mechanisms. The first category includes lithium intercalation compounds ($MP_y \leftrightarrow Li_xMP_y$) that maintain their original structure. Cho et al. reported that lithium intercalation in $SnP_{0.94}$ without changing the Sn oxidation state and 4.5 mol of lithium ion can be intercalated into a $SnP_{0.94}$ structure [13]. The second category includes lithium alloying compounds ($MP_y \leftrightarrow$ M(or Li_xM) + Li_xP). Most metal phosphides compounds such as Sn_4P_3 [10–11], FeP_2 [16] and CoP_3 [19] exhibited lithium alloying and decomposition reactions. These materials showed rapid capacity fading due to particle pulverization from volume expansion and the formation of poor conductor LiP. Kim et al. reported that tin phosphides (Sn_4P_3) with a layered structure prepared by mechanochemical synthesis retained a fairly high reversible capacity in a limited voltage region [10].

The use of ternary tin alloys by introducing another transition metal without reaction with lithium instead of pure tin and binary tin alloys would offer better cycle performance because of the suppression of volume changes during lithium insertion [27–29]. While active materials can react with lithium, non-active materials can buffer the volume change and suppress the aggregation of tin caused by the active compounds. Mao et al. reported various intermetallic phases of Sn and Fe with an active/inactive matrix. In this

* Corresponding authors. Tel.: +82 55 280 1665; fax: +82 55 280 1590.
E-mail addresses: gjpark@keri.re.kr (G. Park), sangma@keri.re.kr (S.-M. Lee).

0925-8388/$ - see front matter © 2014 Published by Elsevier B.V.
http://dx.doi.org/10.1016/j.jallcom.2013.11.082

intermetallic phase, Sn acts with lithium as a reactant, whereas Fe acts as an inactive matrix without reaction with lithium [27].

In this work, we developed a new Fe-substituted Sn_4P_3 alloy to improve the structural stability and electrochemical properties with the concept of an active/inactive alloy in the ternary Sn–Fe–P alloy compound after decomposition reactions. We prepared Sn_4P_3 and $Sn_{3.95}Fe_{0.05}P_3$ alloys by the solvothermal method using tin, iron metal, amorphous red phosphorus as starting materials. We investigated the differences in physical and electrochemical properties between Sn_4P_3 and $Sn_{3.95}Fe_{0.05}P_3$, examined using powder X-ray diffraction, SEM and TEM. We also investigated the electrochemical behavior of Sn–P and Sn–Fe–P compounds using a galvanostatic charge–discharge test, considering the influence of Fe substitution.

2. Experimental

Commercialized tin metal powder (99.0%, Junsei Chemical Co. Ltd.), iron metal powder (98.0%, Duksan Pure Chemical Co. Ltd.), amorphous red phosphorous (98.0%, Kanto Chemical Co. Ltd.) and ethylenediamine (1,2-diaminoethane, anhydrous, 98.0%, Samchun Pure Chemical Co. Ltd.) were used as starting materials for the solvothermal synthesis of tin–iron phosphide. Appropriate amounts of tin metal and red phosphorous were mixed with 60 cm^3 of ethylenediamine in a polytetrafluoroethylene (PTFE) vessel (volume: 100 cm3); the vessel was then capped with a PTFE cover and placed inside a stainless steel reactor. The reactor was sealed and maintained at 200 °C for 20 h. The product of the solvothermal process was collected by filtration, washed four times with distilled water and once with ethanol, and then dried at 100 °C in air. To remove the admixture of metallic tin and red phosphorous from the as-produced samples, the product was washed with vigorous stirring in 0.1 mol/L HCl aqueous solution for 12 h.

Powder X-ray diffraction (XRD, X-pert PRO MPD, Philips, Holland) was carried out with Cu Kα radiation to identify the crystalline phases of the obtained materials. The morphology and particle size of the materials were observed using a scanning electron microscope (FE-SEM, S-4800, Hitachi, Japan). High-resolution transmission electron microscopy (HRTEM, 2100F, JEOL, Japan) equipped with energy-dispersive X-ray spectrometer was used to characterize the micro structure of powders. The TEM samples were prepared using a Focus ion beam (FIB) instrument.

The electrochemical characterizations were performed using a CR2032 coin-type cell. The Sn–P and Sn–Fe–P electrodes were prepared by mixing 80 wt% active material, 10 wt% super P conducting agent and 10 wt% Polyamide imide (PAI, Solvay Advanced Polymer) binder dissolved in N-methyl-2-pyrrolidinone (NMP). The slurry was coated on a copper foil and then dried in a conventional oven at 100 °C for 1 h. The cells were made of a lithium metal anode separated by polypropylene film. The electrolyte was a mixture of 1 M $LiPF_6$-ethylene carbonate (EC)/diethylene carbonate (DEC)/dimethyl carbonate (DMC) (3:5:2 by vol) with 10 wt% fluroethylene carbonate (FEC). The charge and discharge rate was both 0.1 C (0.3 mA/cm^2) with a cut-off voltage of 5 – 2000 mV.

3. Results and discussion

In this study, Sn–P and Sn–Fe–P were prepared via the solvothermal method using tin, iron metal, amorphous red phosphorous and ethylenediamine as starting materials and a N-chelating agent. In general, the pure Sn_4P_3 phase is difficult to obtain due to unreacted metallic tin as an impurity in the reaction and the molar ratio of metal and red phosphorous is a critical factor for obtaining a high yield of the Sn_4P_3 phase using the solvothermal process. In previous studies, when stoichiometric amounts of tin and red phosphorous are applied, the unreacted metallic tin remained in the obtained powder [30–32]. Thus, we applied twice of red phosphorous to the metal in this reaction to obtain a pure Sn_4P_3 alloy compound. Fig. 1 shows the typical XRD results of (a) Sn_4P_3 and (b) $Sn_{3.95}Fe_{0.05}P_3$ alloy powders prepared by solvothermal method. All peaks of the samples obtained by solvothermal synthesis could be indexed as the rhombohedral Sn_4P_3 phase of R3 m (JCPDS#071-2221) with a small mixture of metallic tin (JCDPS#072-3240). These compounds are a layered structure consisting of Sn or Sn and Fe layers and P layers located alternately. No other obvious diffraction peaks arising from impurities such as Fe complex can be detected. This means that the Fe ion cannot change and successfully entered the basic Sn_4P_3 structure. By substituting Sn with

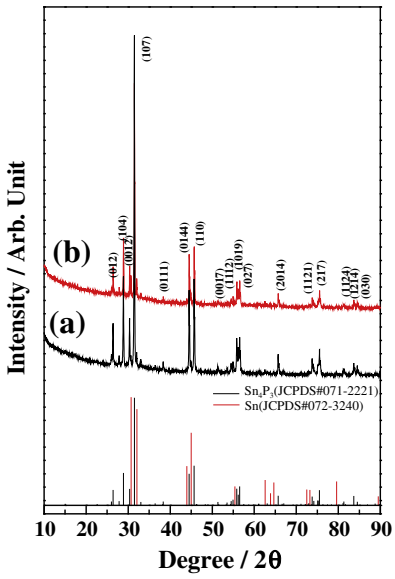

Fig. 1. The XRD results of (a) Sn_4P_3 and (b) $Sn_{3.95}Fe_{0.05}P_3$ alloy powders prepared using the solvothermal method.

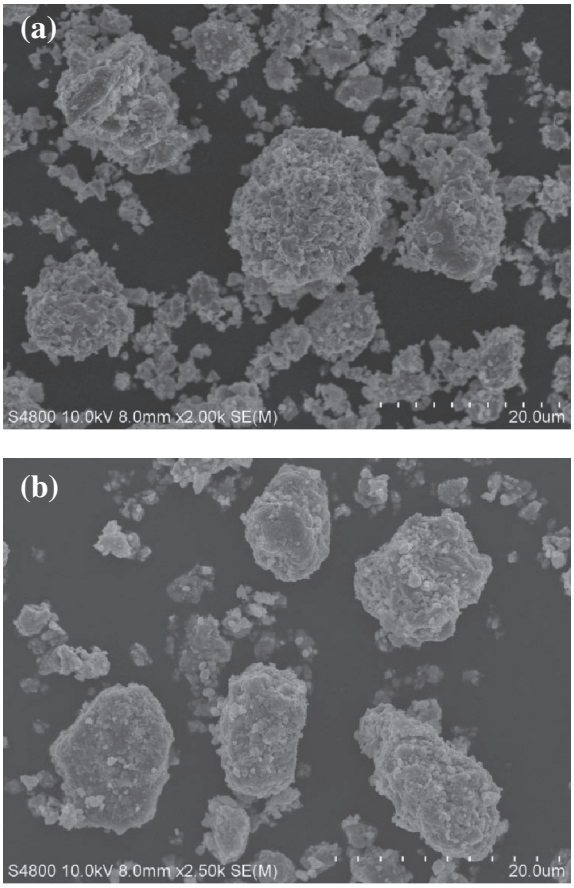

Fig. 2. SEM images of the (a) Sn_4P_3 and (b) $Sn_{3.95}Fe_{0.05}P_3$ alloy powders prepared using the solvothermal method.

Fe, the intensity of the Sn_4P_3 peaks are slightly weakened and the intensity of metallic tin is increased compared to that of pristine Sn-P alloy, indicating the reduction of the average crystallite size of Sn_4P_3. The changes in intensity of these peaks assure that

Fe ion has been successfully substituted in the Sn_4P_3 crystal without any other impurities.

Fig. 2 shows the SEM images of (a) Sn_4P_3 and (b) $Sn_{3.95}Fe_{0.05}P_3$ alloy powders prepared using the solvothermal method. The as-prepared Sn_4P_3 and $Sn_{3.95}Fe_{0.05}P_3$ alloy powders were made of particles with an average size ranging from 1 to 20 μm. All samples also consisted of irregular agglomerated particles where the small particles of 1 – 2 μm size are attached to the edge of large particles of about 10 – 20 μm. The $Sn_{3.95}Fe_{0.05}P_3$ alloy powder has smaller agglomerated particles than the original Sn_4P_3 alloy powder.

Fig 3a and c shows low magnification images of the TEM samples obtained from the Sn_4P_3 and $Sn_{3.95}Fe_{0.05}P_3$ anode materials, respectively, using a focused ion beam (FIB) instrument. The EDS spectra obtained from several locations on the TEM samples were analyzed quantitatively and the atomic concentration profiles are shown as a function of the mapping point in Fig. 3b and d, which shows the uniform distribution of the Sn, P and Fe elements through the samples. The atomic concentrations of each element are shown distributed along the dotted lines in Fig. 3b and d, corresponding to the atomic fraction of each element in the Sn_4P_3 and $Sn_{3.95}Fe_{0.05}P_3$ alloy. In the case of Sn_4P_3, a large amount of P was found on the surface (point 1), but Sn_4P_3 formed uniformly from 2 to 10 point. On the other hand, the $Sn_{3.95}Fe_{0.05}P_3$ alloy formed uniformly at all points. It is confirmed from the XRD and TEM/EDS analysis that the samples have uniform and homogeneous compositions without a secondary phase or inclusion.

Fig. 4 shows bright field and high resolution TEM images of the Sn_4P_3 and $Sn_{3.95}Fe_{0.05}P_3$ samples. The diffraction patterns shown in the insets were obtained by Fourier transformation of the lattice images. The patterns were analyzed in order to index the diffraction spots and the beam directions were obtained from the analysis as indicated in Fig. 4b and e. Fig. 4c and f are simulated diffraction patterns calculated from the beam directions. Fig. 4b and e shows clear lattice point images which represent the well crystallized grains of the Sn_4P_3 and $Sn_{3.95}Fe_{0.05}P_3$ alloys. From these results, it is shown that Fe ion was successfully substituted on the original Sn_4P_3 layered structure without any structural changes.

Fig. 5 shows the charge–discharge curves of (a) Li/1 M $LiPF_6$-EC/DEC/(DMC (3:5:2 by vol) with 10 wt% FEC/Sn_4P_3 and (b) Li/1 M $LiPF_6$-EC/DEC/(DMC (3:5:2 by vol) with 10 wt% FEC/$Sn_{3.95}Fe_{0.05}P_3$ half cells. The test conditions were a rate of 0.1 C with cur-off voltage from 2 to 0.005 V. The electrochemical behaviors between Sn_4P_3 and $Sn_{3.95}Fe_{0.05}P_3$ alloy electrodes are only slightly different to the voltage profiles. For the Sn_4P_3 alloy electrode, the voltage rapidly dropped to 1.25 V and then decreased slowly to 0.70 V at the first discharge process, indicating side reactions between the surface of Sn_4P_3 and the electrolyte. In the Sn_4P_3 synthesized by solvothermal reaction, it was possible to retain the organic residues in its surface due to the starting materials of the organic solvents [31]. After this reaction, the Sn_4P_3 sample showed three voltage plateaus at around 0.7, 0.4 and 0.1 V during the first discharge process which could have contributed to the electrochemical reactions between the Sn_4P_3 electrode and lithium. Three voltage sloping plateaus in the first charge process were observed at around 0.4, 0.6 and 1.1 V. In the subsequent cycles, the charge curves became sharp and moved to higher voltage regions, while the lower potential of the discharge plateaus decreased. This means that the polarization of the electrode has severely taken place depending on the cycle progresses. The initial discharge and charge capacities of Sn_4P_3 are 1739, 1181 mAh g^{-1}, respectively, showing coloumbic efficiency of about 68%. On the other hand, $Sn_{3.95}Fe_{0.05}P_3$ shows a voltage plateau at around 1.0 V for the first discharge process, which results from the reduction of oxide compound on the surface of the $Sn_{3.95}Fe_{0.05}P_3$ compound

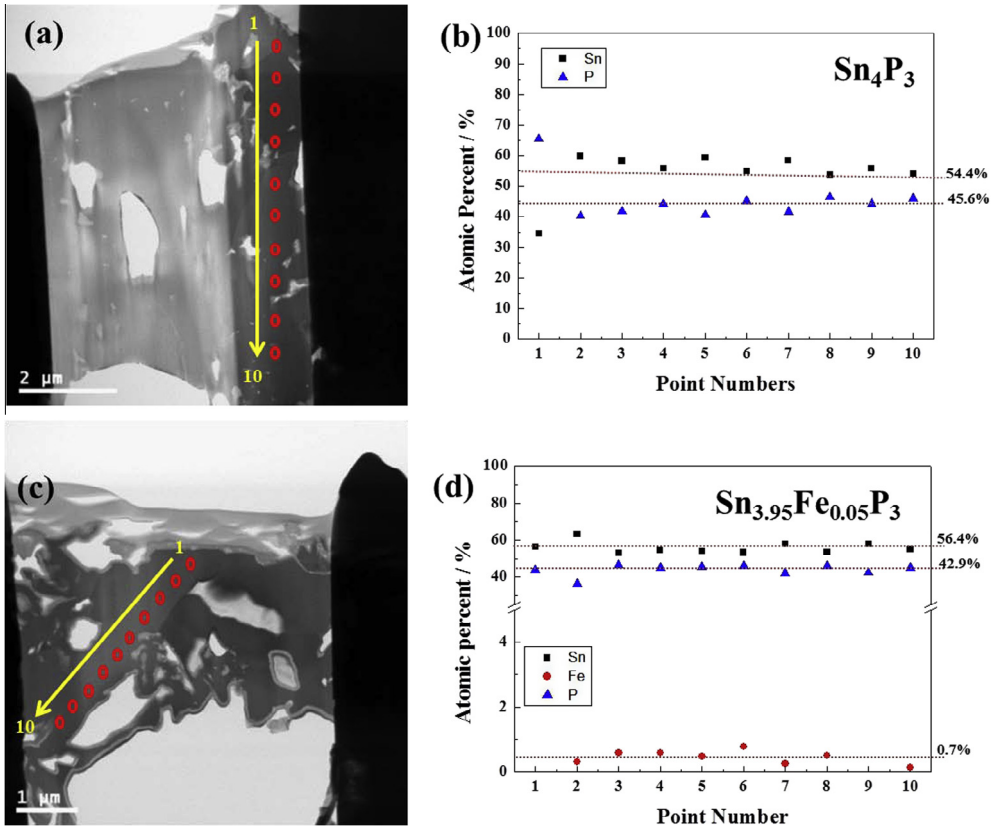

Fig. 3. (a and c) TEM images with EDS point mapping location numbers and (b and d) concentration profiles of (a and b) the Sn_4P_3 and (c and d) $Sn_{3.95}Fe_{0.05}P_3$ samples obtained from EDS analysis on the TEM samples prepared using FIB.

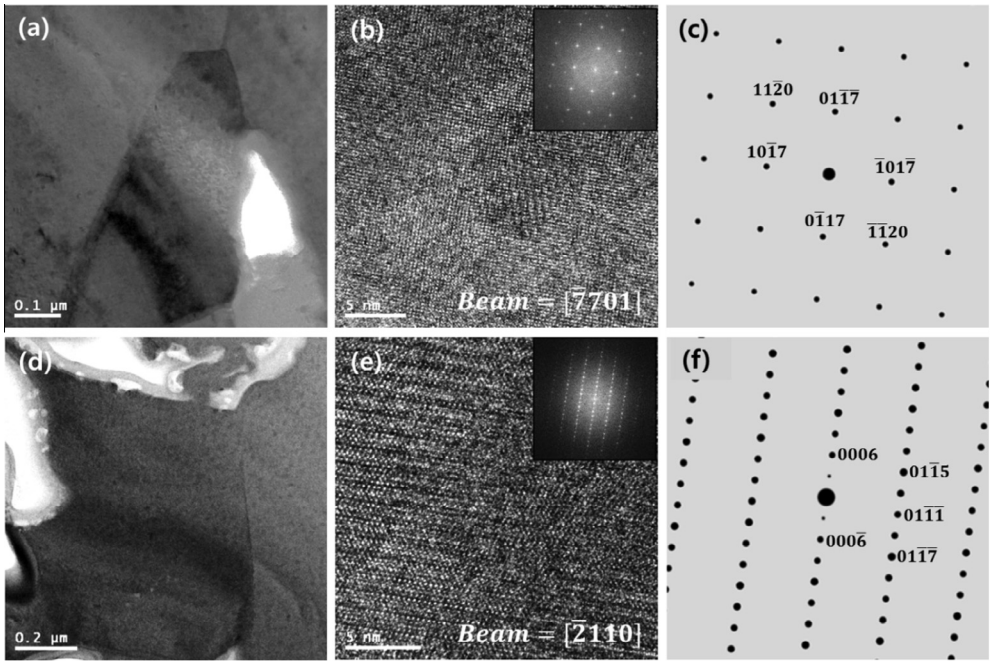

Fig. 4. (a and d) Bright field and (b and e) high resolution TEM images of the (a–c) Sn_4P_3 and (d–f) $Sn_{3.95}Fe_{0.05}P_3$ samples with the inset diffraction patterns obtained by Fourier transformation of the lattice images and (c and f) their simulated patterns.

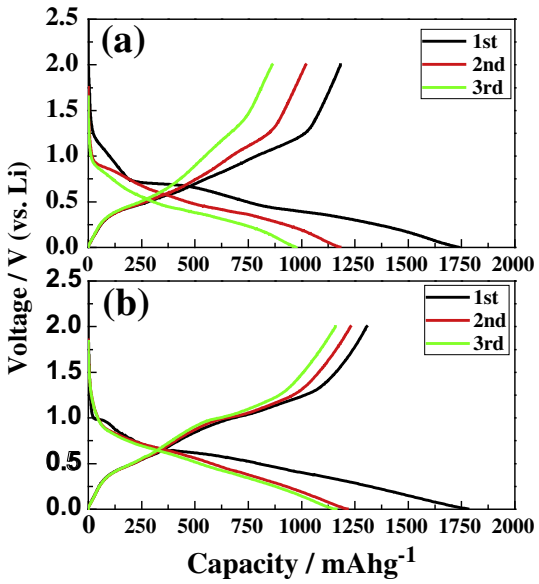

Fig. 5. The charge–discharge curves of (a) Li/1 M $LiPF_6$-EC/DEC/DMC (3:5:2 by vol) with 10 wt% FEC/Sn_4P_3 and (b) Li/1 M $LiPF_6$-EC/DEC/DMC (3:5:2 by vol) with 10 wt% FEC/$Sn_{3.95}Fe_{0.05}P_3$ half cells.

[33]. After this voltage plateau was reached, two voltage sloping plateaus in the first charge process were observed at around 0.6 and 0.4 V. In the charge process, three voltage slope plateaus were shown at around 0.4, 0.6 and 1.1 V. The voltage plateau at 1.0 V of the discharge curves disappeared in the subsequent cycles and maintained linear voltage shapes. The polarization of the electrode was much less than that for the Sn_4P_3 material. The initial discharge and charge capacities of $Sn_{3.95}Fe_{0.05}P_3$ are 1780, 1304 mAh g^{-1}, respectively, showing a coloumbic efficiency of about 73%. The $Sn_{3.95}Fe_{0.05}P_3$ anode material exhibited higher reversible capacity and coulombic efficiency at the first cycle than that of the Sn_4P_3 anode.

To clarify the difference in the reaction and voltage profiles during the charge–discharge process between the Sn_4P_3 and the $Sn_{3.95}Fe_{0.05}P_3$ alloy materials, a differential capacity as the function of potential was converted on the basis of the charge–discharge curves for the Sn_4P_3 and the $Sn_{3.95}Fe_{0.05}P_3$ alloy materials. Differential capacity plots as the function of potential for the (a) Sn_4P_3 and (b) $Sn_{3.95}Fe_{0.05}P_3$ alloys are shown in Fig. 6. Cells were galvanostatically discharged and charged at a current rate of 0.1 C. For the Sn_4P_3 alloy in our study, three peaks were observed at about 0.71, 0.42 and 0.37 V and three broad peaks were observed at about 0.44, 0.56 and 1.0 V, respectively, during the initial discharge and charge process. Kim et al. reported that the Sn_4P_3 anode has three step reaction mechanisms as follows: (1) lithium insertion into the Sn_4P_3 structure (2) formation of various Li_xP and metallic tins and (3) formation of Li_3P and Li_xSn [10,34]. Lithium intercalation into the original Sn_4P_3 layered structure without any structure changes up to 0.8 V. The peak at 0.71 V corresponds to the reaction between lithium and phosphorous, formed by Li_xP. The second and third peaks at 0.42 and 0.37 V are due to the further reactions between lithium, phosphorous and tin. During the charge process, the lithium is extracted from the Sn–Li alloy below 0.7 V and converted from Li_3P to LiP above 0.7 V. In the subsequent cycles, the peak at 0.7 V disappeared and appeared at 0.87, 0.43 and 0.37 V and at 0.44, 0.56 and 1.0 V during the discharge and charge processes, respectively. Surprisingly, $Sn_{3.95}Fe_{0.05}P_3$ alloy has four peaks at about 1.0, 0.64, 0.4 and 0.35 V and at about 0.46, 0.57, 1.0 and 1.2 V during the initial discharge and charge processes, respectively. The peak at 1.0 V is probably due to the reduction of oxide material made by the synthesis process. The second peak at 0.64 V corresponds to the reaction between lithium and phosphorous, which has a lower voltage than that of the Sn_4P_3 alloy. This means that the Sn–P bond in the hexagonal layered structure of $Sn_{3.95}Fe_{0.05}P_3$ was broken below 0.7 V in the first discharge process. The further reaction after this peak in the $Sn_{3.95}Fe_{0.05}P_3$ alloy is almost the same during the discharge process. However, a newly sharpened peak at 1.0 V is observed in the initial charge process and the peak at 0.64 V in the first discharge split into two peaks at 0.84 and 0.66 V during the second discharge process. One of

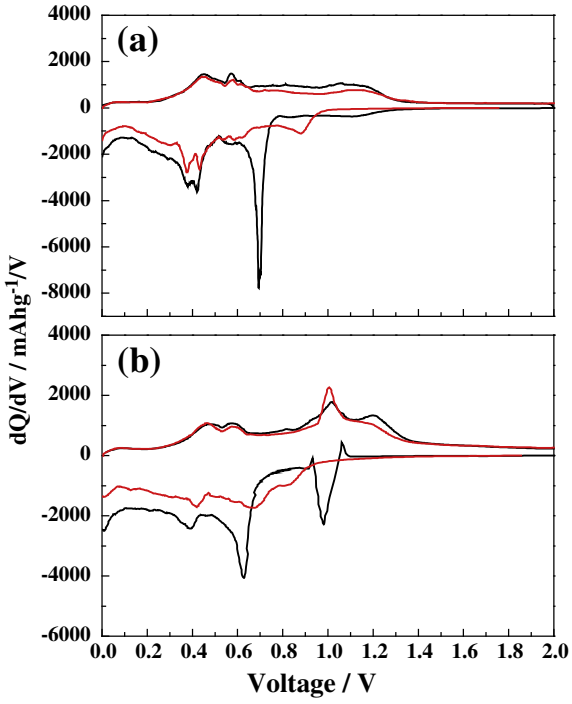

Fig. 6. Differential capacity plots as a function of potential for the first cycle and second cycle of (a) Sn_4P_3 and (b) $Sn_{3.95}Fe_{0.05}P_3$ alloys.

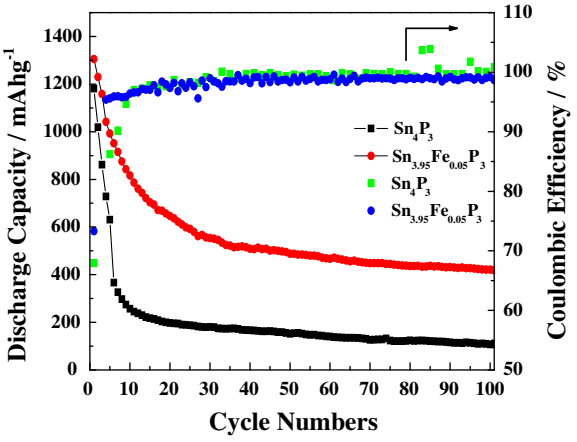

Fig. 7. Cycle performances and coulombic efficiencies of (a) Sn_4P_3 and (b) $Sn_{3.95}Fe_{0.05}P_3$ alloys.

the reasons for the cycling fade of Sn_4P_3 is the irreversibility of the formed LiP phase and the agglomeration of tin atoms, as suggested by Courtney et al. [35]. We assume that, in their Sn–Fe–P structure, Fe ion could have been dispersed between the tin atoms and the agglomeration tin atom could then be suppressed after the decomposition of $Sn_{3.95}Fe_{0.05}P_3$. Voltage profile and differential capacity plots confirmed that Fe ion in the Sn-Fe-P structure could play a role in stabilizing the structure and improving the electrochemical properties during cycling.

Fig. 7 shows the cycle performances and coulombic efficiencies of (a) Sn_4P_3 and (b) $Sn_{3.95}Fe_{0.05}P_3$ alloys. Sn_4P_3/Li showed an initial charge capacity of 1181 mAh g^{-1} and a decrease in the capacity fading of about 200 mAh g^{-1} after the 10th cycle due to the irreversibility of LiP. The capacity of 107 mAh g^{-1} remained after 100 cycles. However, $Sn_{3.95}Fe_{0.05}P_3$/Li showed a high initial capacity of 1304 mAh g^{-1}, showing a coulombic efficiency of 73%. $Sn_{3.95}Fe_{0.05}P_3$/Li also showed capacity fading, but this was smoother than that of the Sn_4P_3 material. It remained at the capacity of 421 mAh g^{-1} after 100 cycles, which is 4 times higher than that of Sn_4P_3. Fe atoms as an inactive matrix could suppress the agglomeration of tin atoms in $Sn_{3.95}Fe_{0.05}P_3$ after the discharge process because it could be dispersed between the tin atoms. The cycling stability was improved and the polarization of the electrode decreased, confirming that Fe substitution in the Sn–P structure is very important to improve the structure stability and electrochemical properties. We are currently conducting detailed studies, including electrochemical and rate performance experiments as well as an investigation of the reaction mechanism and structure change of the $Sn_{3.95}Fe_{0.05}P_3$ alloy during cycling.

4. Conclusion

Sn_4P_3 and $Sn_{3.95}Fe_{0.05}P_3$ alloy materials were prepared via the solvothermal method, using tin, iron, red phosphorous and ethylenediamine. No diffraction peaks were associated with the iron compounds; this suggested that the Fe ion successfully entered the hexagonal layered structure of Sn_4P_3, as observed through the data obtained from the XRD and TEM. The Sn_4P_3 and $Sn_{3.95}Fe_{0.05}P_3$ alloy anodes showed charge capacities of 1181 and 1304 mAh g^{-1}, and the initial coloumbic efficiency was about 68% and 73%, respectively. The $Sn_{3.95}Fe_{0.05}P_3$ anode material exhibited a higher charge capacity and coulombic efficiency at the first cycle than that of the Sn_4P_3 anode. Additionally, the relatively large capacity of about 420 mAh g^{-1} after 100 cycles was achieved in the $Sn_{3.95}Fe_{0.05}P_3$ anode, whereas the Sn_4P_3 anode remained at only about 100 mAh g^{-1} after 100 cycles. The Fe atoms as an inactive matrix could suppress the agglomeration of the tin atoms in $Sn_{3.95}Fe_{0.05}P_3$ after the discharge process because it could be dispersed between the tin atoms. Voltage profile and differential capacity plots confirmed that the Fe ion in the $Sn_{3.95}Fe_{0.05}P_3$ structure could play a role in stabilizing the structure and improving the electrochemical properties during cycling.

Acknowledgement

This study was supported by a National Research Foundation of Korea Grant funded by the Korean Government (MEST) (NRF-2011-C1AAA001-0030538).

References

[1] J.M. Tarascon, M. Armand, Nature 414 (2001) 359–367.
[2] M. Noel, R. Santahnam, J. Power Sources 72 (1998) 53–65.
[3] J.R. Dahn, A.K. Sleight, M. Shi, J.N. Reimers, Q. Zhong, B.M. Way, Electrochim. Acta 38 (1993) 1179–1191.
[4] M. Winter, J.O. Besenhard, M.E. Sphar, P. Novak, Adv. Mater. 10 (1998) 725–763.
[5] M. Yoshio, H. Wang, K. Fukuda, Angew. Chem. Int. Ed. 42 (2003) 4203–4206.
[6] E.J. Pichta, W.K. Behl, J. Power Sources 88 (2000) 192–196.
[7] S.S. Zhang, K. Xu, T.R. Jow, Electrochim. Acta 48 (2002) 241–246.
[8] G. Park, N. Gunawardhana, H. Nakamura, Y. Lee, M. Yoshio, J. Power Sources 199 (2013) 293–299.
[9] G. Park, H. Nakamura, Y. Lee, M. Yoshio, J. Power Sources 189 (2008) 602–606.
[10] Y. Kim, C.K. Lee, H. Sohn, T. Kang, J. Electrochem. Soc. 151 (2004) A933–A937.
[11] Y. Kim, S. Lee, C.K. Lee, H. Sohn, J. Power Sources 141 (2005) 163–166.
[12] J. Wu, Z. Fu, J. Electrochem. Soc. 156 (2009) A22–A26.
[13] Y. Kim, H. Hwang, C.S. Yoon, M.G. Kim, J. Cho, Adv. Mater. 19 (2007) 92–96.
[14] D.C.S. Souza, V. Pralong, A.J. Jacobson, L.F. Nazar, Science 296 (2002) 2012–2015.
[15] S. Sim, J. Cho, J. Electrochem. Soc. 159 (2012) A669–A672.
[16] D.C.C. Silva, O. Crosnier, G. Ouvrard, J. Greedan, A. Safa-Sefat, L.F. Nazar, Electorchem. Solid-state Lett. 6 (2003) A162–A165.
[17] J. Hall, N. Membreno, J. Wu, H. Celio, R. Jones, K. Stevenson, J. Am. Chem. Soc. 134 (2012) 5532–5535.
[18] S. Boyanov, D. Zitoun, M. Menetrier, J.C. Jumas, M. Womes, L. Monconduit, J. Phys. Chem. C 113 (2009) 21441–21452.

[19] V. Pralong, D.C.S. Souza, K.T. Leung, L.F. Nazar, Electrochem. Commun. 4 (2002) 516–520.
[20] R. Alcantara, J.L. Tirado, J.C. Jumas, L. Monconduit, J. Olivier-Fourcade, J. Power Sources 109 (2002) 308–312.
[21] Y. Cui, M. Xue, Z. Fu, X. Wang, X. Liu, J. Alloys Comp. 555 (2013) 283–290.
[22] M. Kim, S. Lee, J. Cho, J. Electrochem. Soc. 156 (2009) A89–A94.
[23] H. Hwang, M. Kim, J. Cho, J. Phys. Chem. C 111 (2007) 1186–1193.
[24] C. Park, Y. Kim, H. Sohn, Chem. Mater. 21 (2009) 5566–5568.
[25] K. Wang, J. Yang, J. Xie, B. Wang, Z. Wen, Electrochem. Commun. 5 (2003) 480–483.
[26] Y. Cui, M. Xue, X. Wang, K. Hu, Z. Fu, Electrochem. Commun. 11 (2009) 1045–1047.
[27] O. Mao, J.R. Dahn, J. Electrochem. Soc. 146 (1999) 423–427.
[28] J.T. Vaughey, J. Owejan, M.M. Thackeray, Electrochem. Solid-State Lett. 10 (2007) A220–A224.
[29] J. Zhang, X. Zhang, Y. Xia, J. Electrochem. Soc. 154 (2007) A7–A13.
[30] K.A. Kovnir, Y.V. Kolen'ko, S. Ray, J. Li, T. Watanabe, M. Itoh, M. Yoshimura, A.V. Shevelkov, J. Solid-State Chem. 179 (2006) 3756–3762.
[31] Y. Xie, H. Su, B. Li, Y. Qian, Mater. Res. Bull. 35 (2000) 675–680.
[32] S. Liu, S. Li, M. Li, L. Yan, H. Li, New J. Chem. 37 (2013) 827–833.
[33] P.A. Connor, J.T.S. Irvine, J. Power Sources 97 (2001) 223–225.
[34] B. Leon, J.I. Corredor, J.L. Tirado, C. Perez-Vicente, J. Electrochem. Soc. 153 (2006) A1829–A1834.
[35] I.A. Courtney, J.R. Dahn, J. Electrochem. Soc. 144 (1997) 2045.